Mechanical Behaviors of Four-Step 1 × 1 Braided Carbon/Epoxy Three-Dimensional Composite Tubes Under Axial Compression Loading

Rotich K. Gideon, Baozhong Sun, Bohong Gu
College of Textiles, Key Laboratory of High Performance Fibers & Products, Ministry of Education, Donghua University, Shanghai 201620, China

This article focuses on the quasistatic axial compression behavior and the consequent energy absorption of three different types of carbon/epoxy braided composite tubes. The focus is to evaluate the effect of sample length and braiding angle on the energy absorption and failure mechanism of the braided composite tubes. All tubes were manufactured with carbon fiber through four-step 1 × 1 braiding process and epoxy resin. Quasistatic axial compression tests were carried out to comprehend the failure mechanism and the corresponding compressive load–displacement characteristics of each braided composite tube. The quasistatic compression test parameters such as the compression peak load and the energy absorption of all these composite tubes were compared. It was found that as the length of the sample increased, the peak load reduced and the energy absorption of the braided tubes at 45° braiding angle was considerably higher than that of other braiding angles of 25° and 35°. The failure modes included matrix crack along the braiding angle, fiber breakage, bulging and debonding between yarns. POLYM. COMPOS., 37:3210–3218, 2016.

INTRODUCTION

The utilization of fiber reinforced composite tubes is ever expanding in aerospace, transport, civil, and structural industries especially due to their high strength-to-weight ratio and energy absorption capabilities when subjected to axial compression loading. The ability to be tailored to give a specific energy absorption capacity, high specific mechanical properties for example stiffness and strength with great design flexibility are other advantages driving the use of reinforced composites. Of these fiber reinforced composites, 3-dimensional (3D) structures have been gaining momentum because of their strength in the entire three axis of the structure (*x*-, *y*-, and *z*-axis). Several manufacturing processes have been used to produce these 3D structures. Weaving, knitting, nonwoven and braiding are the techniques that have been used to produce these structures. In this work, four-step 1 × 1 braiding process was used to produce tubular preform for composite reinforcement. The braiding set up determines the tube geometries, for instance, the inner radius of the braided preform is determined by the mandrel used but the outer radius is determined by the yarn size, yarn jamming and other braiding characteristics [1].

Several researchers have studied the behavior of composite tubes under axial compression loading with different cross-sectional area like squares [2], conical shapes [3], and radial corrugated composite tubes [4], especially for their energy absorption property. Chui et al. studied the energy absorption capability of carbon/epoxy and Kevlar/epoxy square tubes. They observed that constituent material mechanical properties, specimen dimension and the test dynamics influences the crush failure of composite tubes [2]. The progressive end crushing of the square cross section tubes are initiated with crack formation at the corners due to local stress concentration, therefore circular cross section samples exhibits higher energy absorption and progressive crush happens at a superior stress level [5, 6]. In addition, the geometry [7] and the fiber content [8] of the composite tubes play a considerable role in the failure mechanism exhibited. Failure of composite tubes under axial compression has been classified into five failure morphologies: splaying, matrix fragmentation [9], fragmental fracture, progressive folding, and disastrous failure. These failure modes and energy absorption are greatly influenced by the braiding parameters [10, 11], fiber and matrix properties [6, 9, 12, 13] in

Correspondence to: B. Gu; e-mail: gubh@dhu.edu.cn
Contract grant sponsor: National Science Foundation of China; contract grant number: 11272087; contract grant sponsor: National High-tech R&D Program of China (863 Program); contract grant number: 2012AA03A206; contract grant sponsor: Foundation for the Author of National Excellent Doctoral Dissertation of PR China (FANEDD); contract grant number: 201056; contract grant sponsor: Shanghai Science and Technology innovation action plan; contract grant numbers: 12521102400 and 12dz1100407; contract grant sponsor: Fundamental Research Funds for the Central Universities of China.
DOI 10.1002/pc.23519
Published online in Wiley Online Library (wileyonlinelibrary.com).

TABLE 1. Materials properties.

Materials	Tensile strength (MPa)	Tensile modulus (GPa)	Strain (%)	Density (g/cm^3)	Diameter (μm)	Linear density (Tex)
Carbon fiber (T700-12K)	4,900	230	2.1	1.80	7	800
Epoxy resin (JC-02A)	65	2.25	5	1.13	—	—

addition to the trigger mechanisms [5, 11, 14, 15]. Considering braided structures, apart from the braiding angle influencing the capacity of braided composites to carry the axial compression load; it also controls the failure mode and energy absorption capacity of the composite structure [10].

Both the dynamic crushing tests and quasistatic compression tests have been studied. Energy absorption reliance on the rate of loading has been studied and it is connected to the failure mechanism [16, 17]. By opting for suitable compression speeds, quasistatic tests could present significant information concerning the energy absorption capacity and failure mechanisms of composite structures under axial compression loading [6].

Although there is vast collection of literature, across the years, on the subject of the behavior of 3D composite tube materials under axial compression loading, there is need for continuing study on the same because of the new material advancement and manufacturing processes. The aim of this article is to study the axial compression loading behaviors of four-step 1 × 1 braided carbon/epoxy composite 3D circular tubes with different braiding angles. With the aim of achieving this goal, this article endeavors to draw the connection between the compression parameters with sample length and the braiding angle. Three different kinds of circular tubes were fabricated and tested under quasistatic axial compression loading. The compressive load–displacement curves were examined and the compression parameters deliberated based on these curves. The damage mode was observed in order to establish the failure morphology of the compressed tubes.

EXPERIMENTAL

Materials

Carbon fiber was used for preform braiding and it was supplied by TORAYCA®. The fiber was of T700S-12K type and its properties are listed in Table 1. Braiding was done by the actions of the yarn carriers in the length of the row and column tracks. This was the four-step 1 × 1 braiding process which has four row-and-column actions in a braiding sequence which makes the yarns to criss-cross in space as shown in Fig. 1. After the four steps as indicated in the Fig. 1, a yarn end is moved from one bed to another in one direction to ensure that yarn circulate around the braided preform. The braided preform takes the form of $(M \times N) = (2 \times 40)$, where M is the number of columns while N is the number of radial rows. The number of carbon fiber ends used was 120 and it was not changed for all the preforms braided. The ends number used can be calculated from the value of M and N by using *Eq. 1*.

$$\text{Ends} = ((M+1)\times N). \quad (1)$$

Yarn jamming (tightening) step was applied upon each four-step braiding sequence to give a predetermined length and braiding angle of the preform. The yarn structure braided replicated itself in the consecutive sequences. Three braiding angle samples were manufactured, i.e., 45°, 35°, and 25° by changing the yarn jamming strength and four length-to-diameter ratios (L/D) of 1, 2, 3, and 4 were tested.

The braided preform was impregnated with epoxy resin by vacuum assisted resin transfer method (VARTM) inside a tube mold as shown in Fig. 2. The resin was supplied by Changshu Jiafa® Chemical Co. Ltd. and its properties are listed in Table 1. A release paper was wrapped on all molds for easy removal of the tubes from the molds, besides a mold release wax was applied on to the mold surface and also, after the release paper. The impregnation process was done at a temperature of 40°C to aid in faster movement of resin through the preform by lowering its viscosity. Curing was done in steps of 90°C for 2 h, 110°C for 1 h, and finally 130°C for 4 h.

The test specimens were cut adequately short to evade Euler's buckling and yet sufficiently long enough to permit any stress concentration at the boundary to disintegrate into uniaxial stress condition which acts at the centre of the tube as discussed by Roslan et al. [18]. For each detailed type of specimen, three tubes were manufactured and tested with the average determined value of each parameter being reported. Figure 3 shows samples of different length in the ratio of diameter but of the same braiding angle. The sample specifications are shown in Table 2. Figure 4 shows samples of same height but of different braiding angles. The specifications of sample with the same height are shown in Table 3.

Axial Compressive Tests

The axial compression test was done on a Universal testing machine MTS® as shown in Fig. 5 according to ASTM 695-02 standards. The samples were subjected to axial compression test, between two tubs shown in Fig. 6, to failure at a rate of 1.3 mm/min. The tubs were used to ensure stability of the samples during tests. This test was done in order to ascertain the fundamental failure mechanisms of the braided tube and the energy absorbed. The tests were carried out devoid of using trigger mechanisms for instance chamfering of the tube ends. Compressive

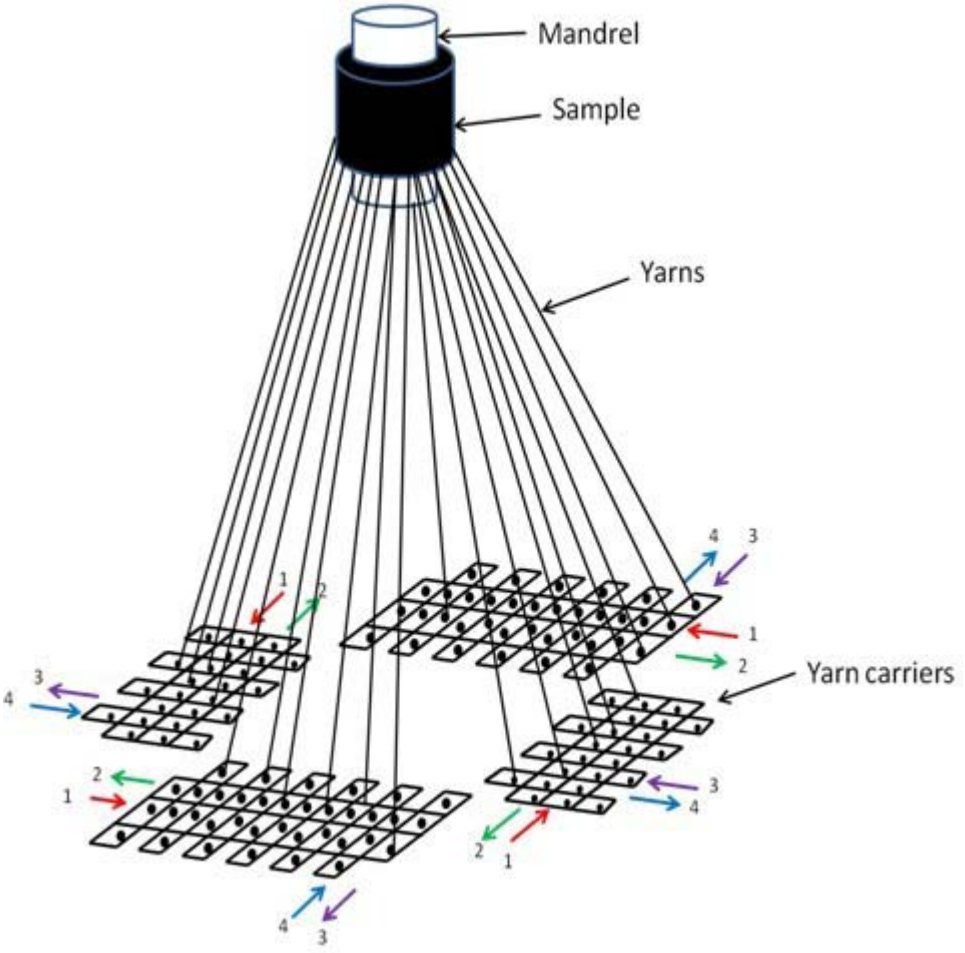

FIG. 1. Four-Step 1 × 1 braiding process with four beds for tubular braiding. [Color figure can be viewed at wileyonlinelibrary.com]

load–displacement curves were obtained during crushing directly from the testing machine. Naturally, the curves demonstrate an increase in load with increase in compression distance up to the sample failure point.

A diagram of a typical compressive load–displacement curve response of a tubular composite under axial quasi-static compression is shown in Fig. 7. The compressive behaviors of a tubular composite can be characterized by

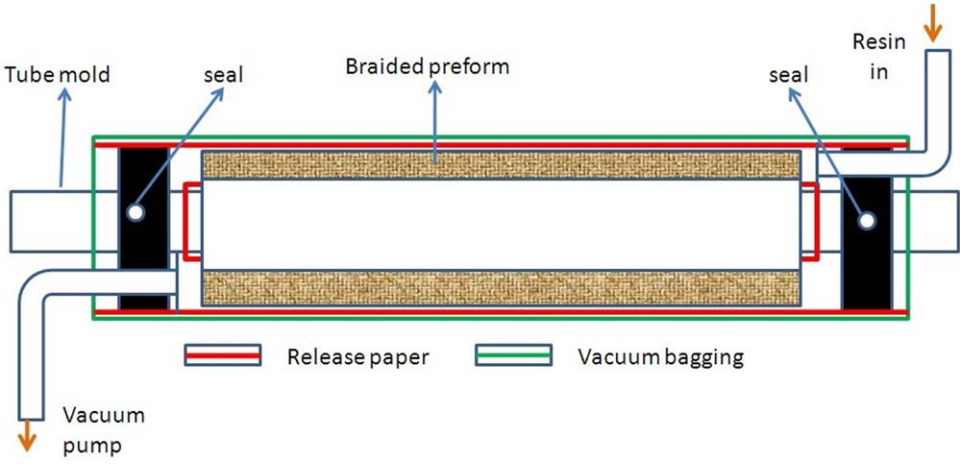

FIG. 2. Vacuum resin transfer molding process. [Color figure can be viewed at wileyonlinelibrary.com]

 DOI 10.1002/pc

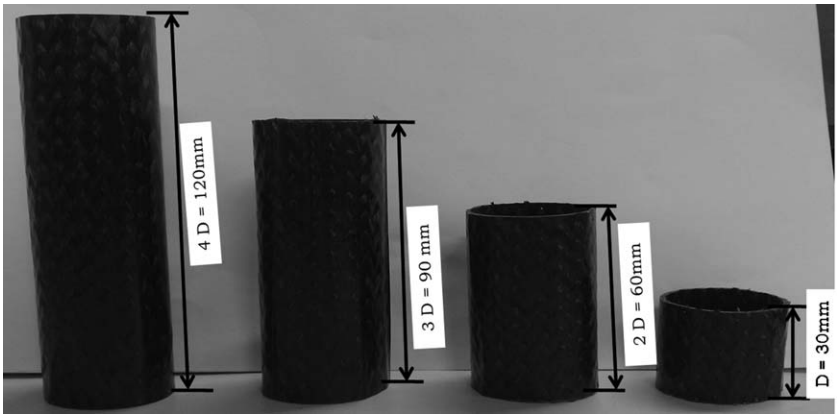

FIG. 3. Samples of different height according to diameter ratio.

use of peak load, average load and energy absorbed by the tube equivalent to the area under the curve. Pictures of the failed samples were taken following the testing process conclusion, with an aim of illustrating the macroscopic features of the failure modes that were observed in the course of the static axial compression on the tubes samples.

RESULTS AND DISCUSSION

Braided Materials

Since braiding was done on a circular mandrel, a tubular preform was braided. Different forces of jamming were used thus three braiding angles were achieved. Higher force of jamming resulted in a higher braiding angle and vice versa. Higher braiding angle had great influence on both geometry and physical properties of the braided preform. As outlined in Table 3, the outer diameter and the thickness of the tube increases as the braiding angle increases. Both the weight and the density of the preform also increased.

TABLE 2. Material specifications for sample of different lengths.

Length (mm)	Ratio to *D*	Braiding angle	Fiber volume fraction (%)	Mass (g)	Peak load (kN)
30	1	25°	39	5.8	22.9
	1	35°	41	7.1	21.13
	1	45°	43.5	8.8	26.53
60	2	25°	39	11.5	21.34
	2	35°	41	14.2	19.95
	2	45°	43.5	17.6	25.3
90	3	25°	39	17.4	19.78
	3	35°	41	21.3	19.5
	3	45°	43.5	26.4	24.7
120	4	25°	39	23.2	18.52
	4	35°	41	28.4	18.17
	4	45°	43.5	35.2	23.51

Results of Test of Same Braiding Angle Samples With Different Lengths

Compressive Load–Displacement Curve. Figure 8 shows the compressive load–displacement curve of samples with the same braiding angle but different height. It can be observed that at the beginning, the load increases linearly with the compression distance, i.e., the tubes act elastically up to the peak load. Subsequently, there is a large drop in the load which coincided with crack initiation. The initial moduli of the curves are equivalent, an evident that changing the length of the tube does not affect the initial modulus. The peak load was influenced by the change in sample

FIG. 4. Samples of same height but different braiding angle. [Color figure can be viewed at wileyonlinelibrary.com]

TABLE 3. Material specifications for sample of different braiding angle.

Braiding angle	Length (mm)	Inner diameter (mm)	Outer diameter (mm)	Mass (g)	Fiber volume fraction (%)	Peak load (kN)
45°	60	30	36	17.7	43.5	25.3
35°	60	30	35	14.2	41	19.95
25°	60	30	34	11.5	39	21.34

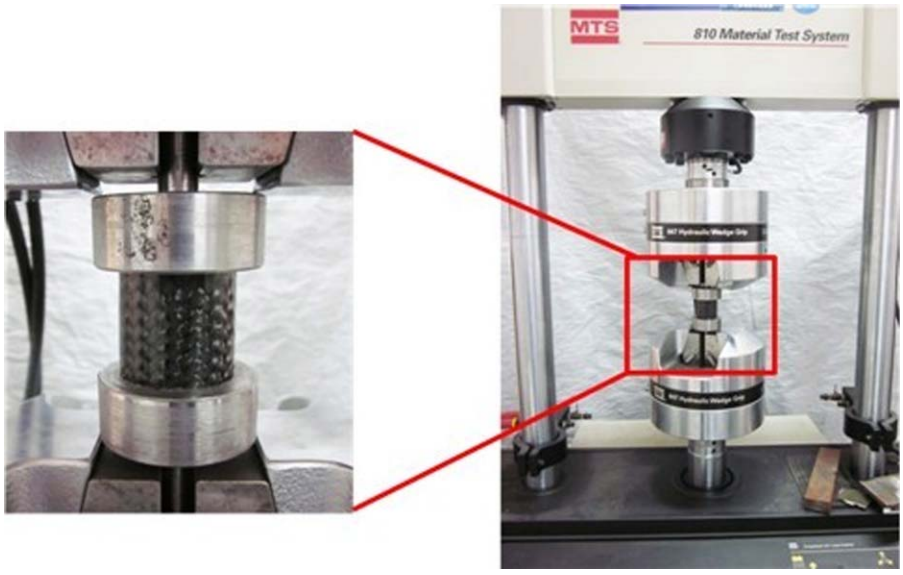

FIG. 5. MTS machine used for axial testing. [Color figure can be viewed at wileyonlinelibrary.com]

height. The tube with the height equal to its diameter had the highest peak load while the tube with the height four times the diameter had the lowest load peak. Undeniably, the extent of the peak load was significantly affected by the ratio of tube length to diameter. Similar conclusion was given by Yan et al. [19] and Eshkoor et al. [20]. From the curves it can be concluded that as the length of the tube is increased, the peak load reduces gradually as shown in Fig. 9. This observation was made from all the tubes with different braiding angles.

Damage Morphology. A significant factor used to evaluate the behavior of the composite tubes under axial compression is the failure mechanism. For samples which fail in a steady progressive mode, the difference of the force as a function of displacement will not be large and for this reason it provides an even deceleration [15]. From Fig. 10, it can be observed that all the samples failed with matrix crack and fiber breakage along the braiding angle. This shows that the load applied to the tubes is distributed by the braiding yarns along the surface of the tube.

As the axial compression load draws near the maximum load of the sample, the creation of cracks begins at the ends of the tubes due to concentration of the local stress. These cracks spread along the yarns following the braiding angle of the tubes followed by a sharp drop of loading stress. Additional spread of these cracks leads to total failure of the tube.

Results of Test of Same Length With Different Braiding Angles

Compressive Load–Displacement Curve. The effect of braiding angle on the peak load is shown in Fig. 11. The tubes with 45° braiding angle had the highest peak load because of higher fiber volume fractions as compared to other specimens. With higher volume fraction, more yarns

FIG. 6. Support base of the tube. [Color figure can be viewed at wileyonlinelibrary.com]

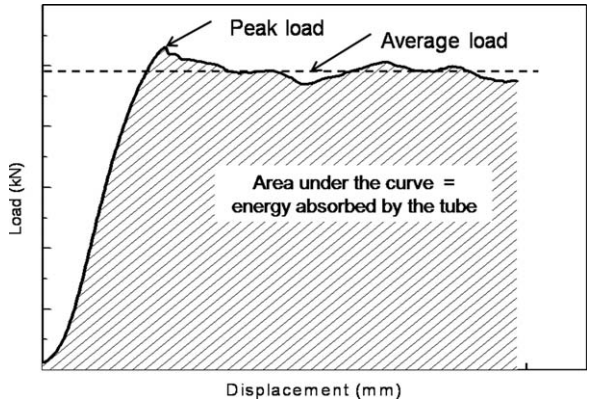

FIG. 7. Typical compressive load–displacement curves response of a tubular composite.

 DOI 10.1002/pc

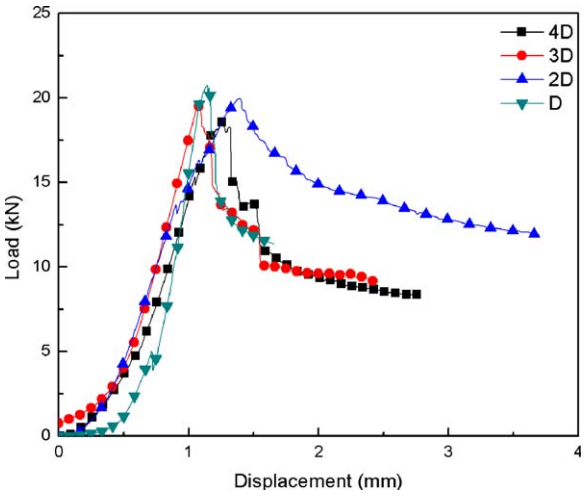

FIG. 8. Compressive load–displacement curves for different heights as compared to diameter ratio ($D = 30$ mm, $2D = 60$ mm, $3D = 90$ mm, and $4D = 120$ mm). [Color figure can be viewed at wileyonlinelibrary.com]

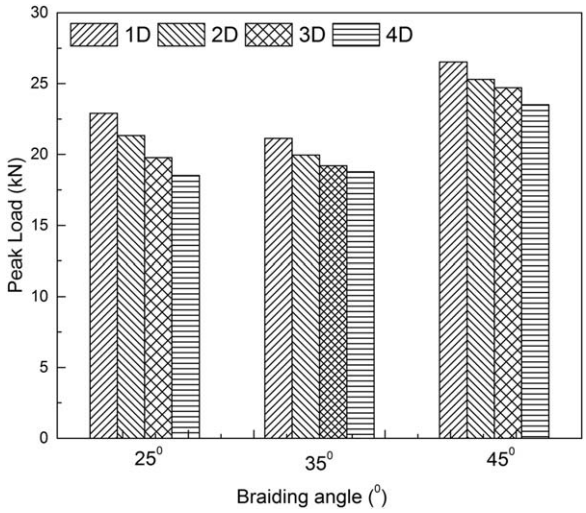

FIG. 9. Peak load–diameter ratio comparison.

carry the load more than the matrix. The second highest peak load was with the samples with 25° braiding angle. This was because at this braiding angle, the fibers were almost on the vertical position meaning that a large component of the fiber compressive strength carried the load. This observation was made in all the different length tested as shown in Fig. 12. The shape of compressive load–displacement curve of braided carbon/epoxy composite tubes under axial compression loading relies on the failure mode. The fracture characteristics of the tubes seemed to influence the values of peak load and the energy absorbed throughout the compression loading process. In contrast with the tubes having braiding angle of 25° and 35°, the tubes with the braiding angle of 45° collapsed in a steady manner with extra resistance and fewer fluctuations in the size of load during the compression loading.

Energy Absorption Capability of Braided Tube. The capacity of a sample to absorb energy can be deduced from the area under the load–compression distance curve. The use of absorbed energy capability is vital when evaluating the capacity of energy absorbers and a larger value means a more efficient energy absorber. Samples of 2D

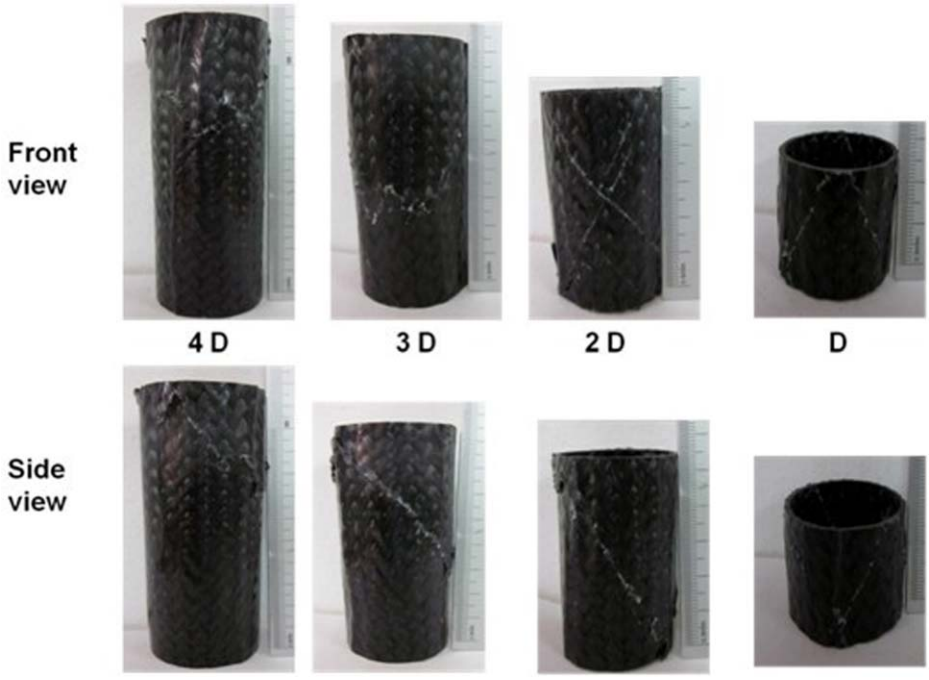

FIG. 10. Damage morphology. [Color figure can be viewed at wileyonlinelibrary.com]

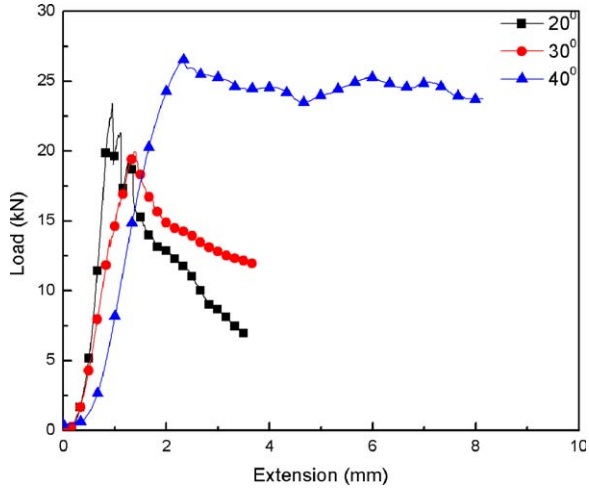

FIG. 11. Compression load-displacement curves of samples of same height (2D = 60mm) with different braiding angles. [Color figure can be viewed at wileyonlinelibrary.com]

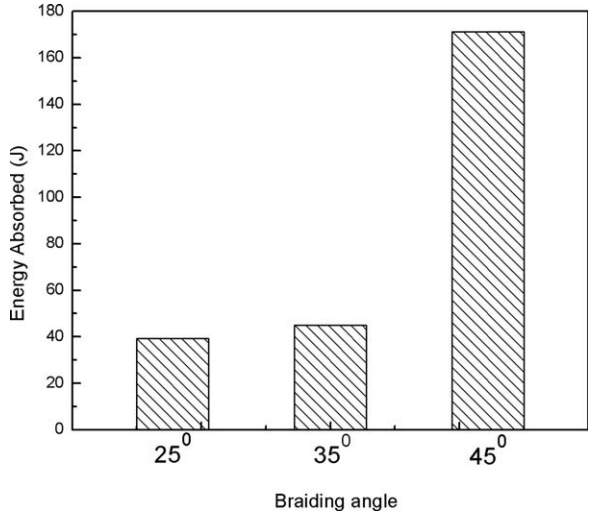

FIG. 13. Energy absorbed by axial compressed tubes of same height of 2D = 60 mm.

length = 60 mm was used to compare the energy absorption of different tubes with different braiding angles. From Fig. 13, it is evident that the tubes with 45° braiding angle absorbed a lot of energy during compression test. As mentioned earlier, the main reasons were because of its higher fiber volume fraction and at the same time, it maintained a constant peak load for a longer duration. This can be understood by the fact that the value of the average load greatly affects the total absorbed energy. The tubes with 25° braiding angle absorbed the least energy because the load increased to the peak value and then dropped sharply to a very low post-failure load without stabilizing into a constant load. The same observation was made on the tubes with 35° braiding angle. By comparing tubes with 25° and 35° braiding angle, the former has a higher peak load but lower energy absorption capability as shown in Fig. 13. It implies that the energy absorption capacity is least influenced by the peak load considering the quantity of energy absorbed by the composite tube under axial compression.

Specific Energy Absorption (E_s). In comparing diverse materials or unlike geometry of samples, it is essential to evaluate the specific energy absorption. The specific energy absorption can be described as the quantity of energy absorbed for every unit mass of compressed material. For this reason, the specific energy absorbed (E_s) that is reliant on the sample geometry was utilized in contrasting the energy absorption 25°, 35°, and 45° braiding angle samples. Specific energy absorption (E_s) can be evaluated using the following equation:

$$E_s = \frac{E_T}{M_S} \tag{2}$$

where E_s is the specific energy absorbed, E_T is the total energy absorbed by the sample, and M_s is the mass of the

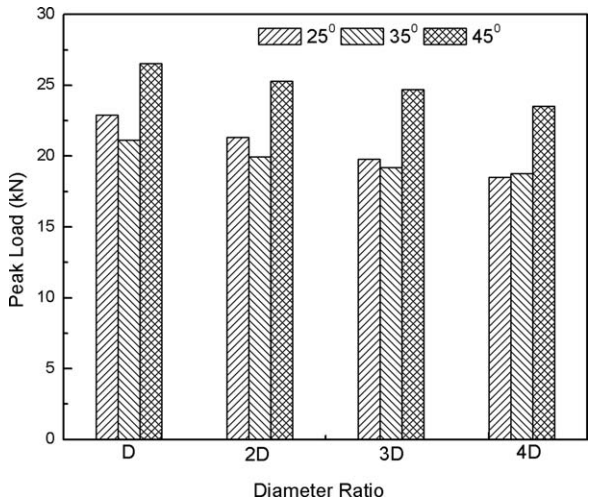

FIG. 12. Peak load–braiding angle comparison.

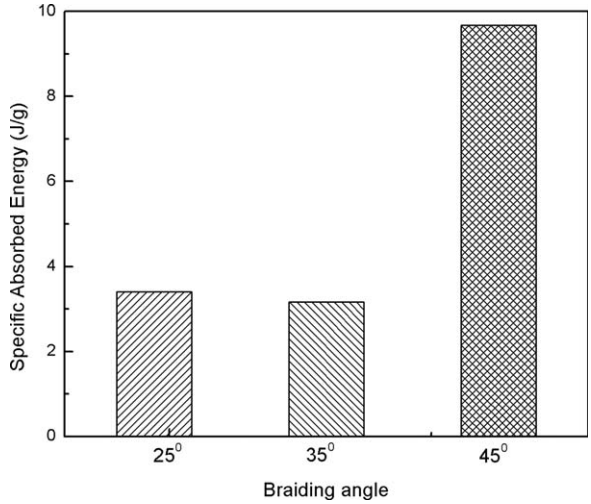

FIG. 14. Specific energy absorbed by tubes of same length (2D = 60 mm) with different braiding angles.

DOI 10.1002/pc

FIG. 15. Damage morphology of samples with different braiding angle. [Color figure can be viewed at wileyonlinelibrary.com]

sample. Figure 14 shows specific energy absorbed by different samples with same height of 2D = 60 mm but different braiding angle. It can be seen that tubes with braiding angle of 45° have high specific energy absorption despite being heavier than other samples. It is followed by 25° and the lowest is 35° braiding angle sample. The reason for this is because of low mass of the 25° braiding angle sample.

Damage Morphology. Four failure modes were observed during the axial compression loading namely: matrix crack, fiber breakage, bulging and debonding between yarns. For tube samples with 25° and 35° braiding angles, they failed by matrix crack and fiber breakage as shown in Figs. 15 and 16, respectively. The crack formation on the tube was followed by an instant plummet of the compressive load [5] and its propagation was along the braiding angle of the tube. For tube samples with 45° braiding angle, as the load increased, the tube wall expanded outward until it failed by bulging as shown in Fig. 15.

Mechanism Analyses on Damage Morphology. Axial compression damage mechanisms of 3D composites tubes can be divided into three parts. In the first part, the composite tube behaves elastically such that as the compression load increases the compressed distance increases up to the peak load. At the second part, i.e., at the peak load, matrix crack starts at the end of the tube due to stress concentration especially for the samples with 25° and 35° braiding angle. The onset of matrix crack coincides with the decline of the compression load. Numerous areas of matrix crack instigation were noticeable and once they were formed, the opposite sides move in different

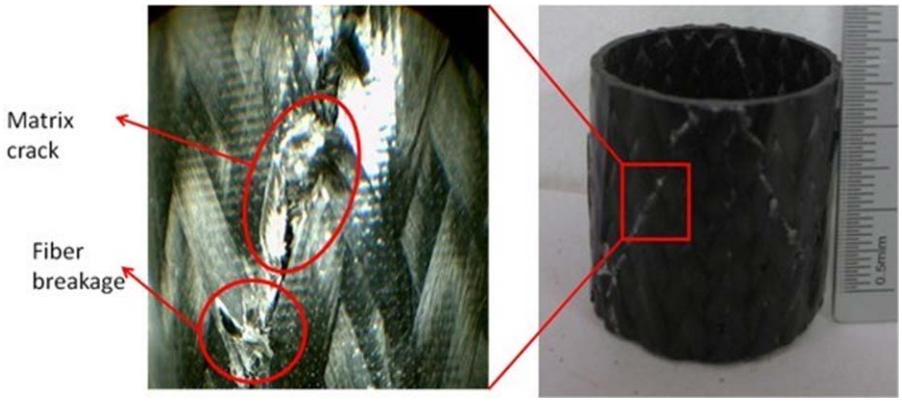

FIG. 16. Failure morphology. [Color figure can be viewed at wileyonlinelibrary.com]

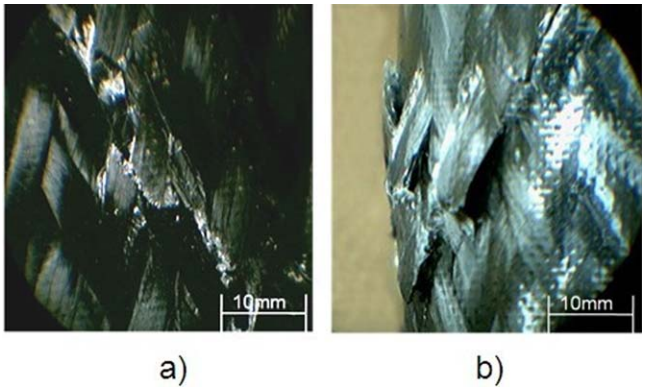

FIG. 17. (a) Matrix crack plus fiber breakage and (b) Debonding between the yarns. [Color figure can be viewed at wileyonlinelibrary.com]

directions leading to shear loading of the yarns which causes yarns brakeage as clearly seen in Fig. 17a. At the joints where two cracks met, debonding between yarns occurred as shown in Fig. 17b. Figure 17a shows crack spreading along the braiding angle which occurs at the third part and when the cracks merge, it leads to composite failure. During the third part, the crack is spread slowly or faster depending on the composite properties. This part also determines the energy absorption capability of the tube in that the slower the crack spreads the higher the energy absorbed by the tube. For tubes with 45° braiding angle, bulging occurred because compression load causes the preform to expand outward. The tube-wall local bulging was started after a significant compressive peak load was attained, which signified the last part of the elastic loading phase and plunging of the load followed.

CONCLUSIONS

The behavior of 3D four-step braided composite tubes has been studied under static axial compression loading. The braiding parameters have been shown to affect both the geometry and the physical properties of the braided composite tube. Yarn jamming strength influences significantly the size of the braiding angle to be braided and in turn influences the tube wall thickness, the outside diameter and the yarn volume fraction. The tube length affects significantly the peak load and subsequently the energy absorption capability of the composite tubes.

It was observed that the tubes with high braiding angle of 45° exhibited high peaked load and high energy absorption. The specific energy absorption levels of the composite tubes increased as the braiding angle increased. The failure modes of all the types of samples were examined and the four failure modes observed during the loading process include; matrix cracking, fiber breakage, bulging and debonding between yarns. The matrix crack was the main dominant failure mode and it occurred along the braiding angle of the braided tube.

REFERENCES

1. Y.Q. Wang and A.S.D. Wang, *Appl. Compos. Mater.*, **4**, 121 (1997).
2. C.H. Chiu, C.K. Lu, and C.M. Wu, *J. Compos. Mater.*, **31**, 2309 (1997).
3. M. Kathiresan, K. Manisekar, and V. Manikandan, *Compos. Struct.*, **108**, 584 (2014).
4. E.F. Abdewi, S. Sulaiman, A.M.S. Hamouda, and E. Mahdi, *Thin Wall Struct.*, **46**, 320 (2008).
5. A.G. Mamalis, D.E. Manolakos, M.B. Ioannidis, and D.P. Papapostolou, *Compos. Struct.*, **69**, 407 (2005).
6. J.D.D. Melo, A.L.S. Silva, and J.E.N. Villena, *Compos. Struct.*, **82**, 622 (2008).
7. S. Palanivelu, W. Van Paepegem, J. Degrieck, D. Kakogiannis, J. Van Ackeren, D. Van Hemelrijck, J. Wastiels, and J. Vantomme. *Polym. Test.*, **29**, 381 (2010).
8. S. Ramakrishna, *J. Reinf. Plast. Compos.*, **14**, 1121 (1995).
9. E. Mahdi, A.M.S. Hamouda, and T.A. Sebaey, *Mater. Des.*, **56**, 923 (2014).
10. C.H. Chiu, K.H. Tsai, and W.J. Huang, *J. Compos. Mater.*, **32**, 1964 (1998).
11. L.J. Gui, P. Zhang, and Z.J. Fan, *Int. J. Crashworth.*, **14**, 17 (2009).
12. S.J. Beard and F.K. Chang, *Int. J. Crashworth.*, **7**, 191 (2002).
13. S. Beard and F.K. Chang, *J. Thermoplast. Compos.*, **15**, 3 (2002).
14. M.R. Schultz and M.W. Hyer, *J. Compos. Mater.*, **35**, 1747 (2001).
15. L. Yan and N. Chouw, *Mater. Des.*, **51**, 629 (2013).
16. A.G. Mamalis, M. Robinson, D.E. Manolakos, G.A. Demosthenous, M.B. Ioannidis, and J. Carruthers, *Compos. Struct.*, **37**, 109 (1997).
17. G.L. Farley, *J. Compos. Mater.*, **25**, 1314 (1991).
18. A. Roslan, M. Zaidi, and M.S. Pasricha, *Pertanika J. Sci. Technol.*, **9**, 219 (2001).
19. L. Yan, N. Chouw, and K. Jayaraman, *Mater. Des.*, **56**, 528 (2014).
20. R.A. Eshkoor, S.A. Oshkovr, A.B. Sulong, R. Zulkifli, A.K. Ariffin, and C.H. Azhari, *Mater. Des.*, **47**, 248 (2013).